Modelling freshwater plume in the Bay of Bengal with artificial neural networks

Dhanya Sumangala, Apurva Joshi and Hari Warrior*

Department of Ocean Engineering and Naval Architecture, Indian Institute of Technology, Kharagpur 721 302, India

In spite of advanced modelling techniques, the current prediction of ocean parameters along the ocean coasts remains a formidable challenge. The traditional methods of using mass and momentum equations to solve the physics of flow have helped us understand the oceans better, but their accuracy remains a problem. This article examines the ability of Delft3D to study freshwater plumes along the northern Bay of Bengal (BoB). Whereas the near shelf is primarily driven by tides and local winds, the far shelf is influenced by the freshwater-driven density circulation and monsoonal ocean currents. The prediction of far shelf waters is well represented by employing an artificial neural network. By tuning the parameters properly, we can better predict the freshwater currents in the BoB with a correlation of 0.957 and 0.986 for *u* and *v* velocities respectively.

Keywords: Artificial neural network, Bay of Bengal, freshwater plume, ocean modelling, multiple linear regression.

COASTAL monitoring is vital in the operational management of ports and harbours, and proper weather prediction plays a major role in this. The weather forecast helps in the smooth movement, berthing and docking of ships and plays a major role in the safety and financial management of ports. Nowadays, weather prediction is made in a timely and routine manner using various ocean and atmospheric models. These models predict the velocity, temperature and wave conditions accurately so that we may use them for further practical applications. Now with tools like machine learning and artificial intelligence, the model-predicted values are more accurate and this is the topic of the present article.

For a one-dimensional (1D) analysis of the development of thermal structures, a 1D turbulence model called the general ocean turbulence model (GOTM) was adopted[1,2]. Regional ocean modelling system (ROMS) and geophysical fluid dynamics lab (GFDL) modular ocean model (MOM) have also been used in real-time prediction. ROMS is a terrain-following, free-surface primitive equations ocean numerical model that solves Reynolds-averaged Navier–Stokes equations using hydrostatic and Boussinesq approximations. Rao and Sivakumar[3] studied the circulation features, storm surges and associated water levels along the Kalpakkam coast, Tamil Nadu, India using an advanced two-dimensional, depth-integrated, finite-element model called ADCIRC. Despite being successful, these models had several limitations related to the assumptions, the lack of initial/boundary conditions and uncertainties regarding other forcing variables. Besides this, parameters like bathymetry, heat exchange, wind drag, etc. are sensitive to the model outcomes.

Recent applications using soft computing, artificial intelligence, machine learning and data mining have been found to handle the complex patterns in the data better[4]. Artificial neural network (ANN) is one such method used here to study the thermohaline circulation in the head Bay of Bengal (BoB). Though the concept of ANN was introduced in the 1940s, it was well-received after several algorithms were proposed for training the data[5]. Wasserman[6], and Bose and Liang[7] have discussed the applications of these neural networks in certain fields.

Several studies described successful applications of ANN on various oceanographic parameters like wave height, wave period, wave direction, tidal levels, sea-level, temperature, wind speed, etc.[8–12]. Deo[17] showed that ANN surpasses several numerical models in terms of result accuracy, in spite of the effort put in for training and structuring the network. Dauji *et al*.[22] showed that very high accuracy in results could be obtained when the networks are properly trained.

In oceanography and coastal engineering, scientists primarily use the feed-forward type of ANN when trained with a more resilient back-propagation algorithm[6,23]. Here, the input data are run through hidden nodes which transform the results using a transfer function[24]. This is fed through multiple hidden layers and appropriate learning skill is developed for the algorithm.

ANNs have the inherent advantage that they are not heavily constrained, as the laws of physics might allow, but are more flexible and adaptive in their applications, especially for coastal velocities[25] and SSTs in ocean engineering. This article deals with the current velocity analysis in the far shelf region using a combination of the numerical model Delft3D and ANN, which is then used to observe the spread of freshwater plumes, a prominent feature of the Northern BoB.

The region of concern in this study is the BoB, which is the northeastern part of the Indian Ocean, encompassed

*For correspondence. (e-mail: warrior@naval.iitkgp.ernet.in)

by a closed boundary in the north, a semi-enclosed East Indian Coastal Current (EICC) boundary in the east and west, and an open boundary in the south (Figure 1). This region experiences freshwater discharge of variable characteristics[26] and magnitude from various rivers such as the Ganges, Brahmaputra, Mahanadi, Krishna and Cauvery[27]. In addition to the high fresh-water input, the BoB is also unique in the seasonal reversing coastal currents[28] and the phenomenon of coastal seasonal upwelling[29,30], which is the motive for the present study.

Materials and methods

Study area

The study area extends from 20° to 24°N and 87° to 92°E, comprising the continental shelf region in the northern BoB. The bathymetry of the region has been taken from GEBCO 08 (Figure 2).

Several rivers discharge into the BoB at a seasonally varying rate (Figure 3)[27]. These outfalls produce a low saline environment in the northernmost bay, with freshwater spread over the continental shelf. Trying to model these coastal waters without taking into account the freshwater density-driven circulation is highly erroneous. So, including these thermohaline circulations in modelling the Bay forms the motivation for this work. Such thermohaline plumes are found in many parts of the world[31].

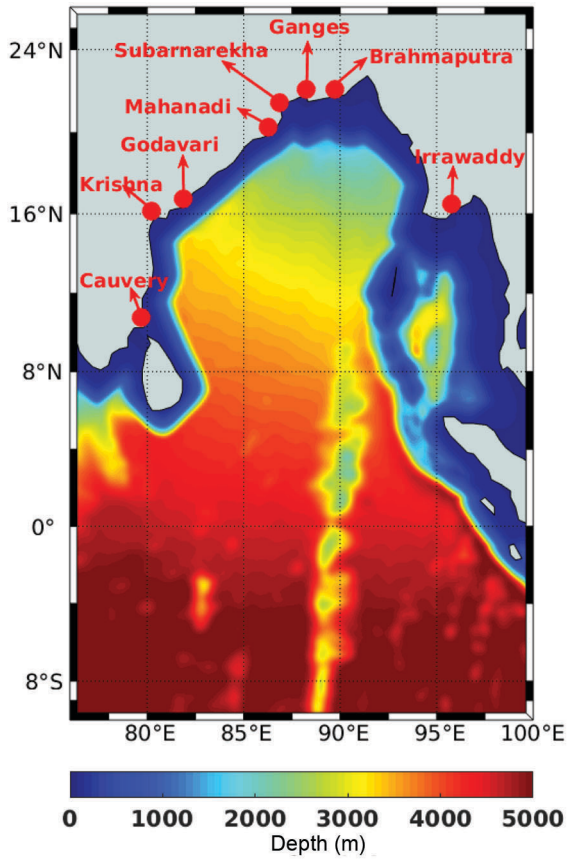

Figure 1. The Bay of Bengal (BoB) with major rivers.

Validation dataset

Ocean surface current–analysis real-time (OSCAR) contains near-surface ocean current estimates derived using quasi-linear and steady-flow momentum equations. It uses data like sea surface heights, surface wind vectors and SST, from several satellites such as TOPEX/POSEIDON altimeters, Jason, Poseidon-2 altimeter, DMSP–F8,10,11 special sensor microwave imager (SSM/I) and several *in situ* instruments to estimate the current velocities. According to Bonjean and Lagerloef[32], the OSCAR data are automatically computed from gridded fields of surface topography and wind derived from the satellite altimeter and scatterometer employing methods developed at Earth and Space Research (ESR), USA. The data have a spatial resolution of one-third degree and temporal resolution of five days.

The open-ocean circulation (basin-scale) in the BoB is highly modulated by seasonal winds (northeast and southwest winds), and it primarily affects the density-driven flow of freshwater plumes. It spreads seasonally, with the EICC carrying it to the southwest during the winter monsoon[33,34] and to the northeast during the summer monsoon. The validation in the far shelf is, therefore, between the OSCAR and Delft3D outputs augmented by ANN. Aydogan *et al.*[35] reported that to determine the oceanographic parameters, one station would suffice for an accurate picture of the shelf.

Numerical model – Delft3D

Delft3D-FLOW is a multi-dimensional, hydrodynamic-transport numerical program which calculates flow that results from tidal and meteorological forcing on a particular grid. In 3D simulations, the vertical grid follows the σ-coordinate algorithm.

The study area was generated with a grid size of 0.01° × 0.01° in the spherical coordinate system with bathymetry.

Table 1. Mesh and input variables for Delft3D

Variable	Details
Bathymetric chart	GEBCO_08
Temperature and salinity	Reynolds and Smith
Wind	QuikSCAT scatterometer
Domain of simulation	20°–24°N; 87°–92°E
Horizontal resolution	0.01°
Vertical resolution	2 m
Domain grids	500 × 405
Tide	TPXO 7.1

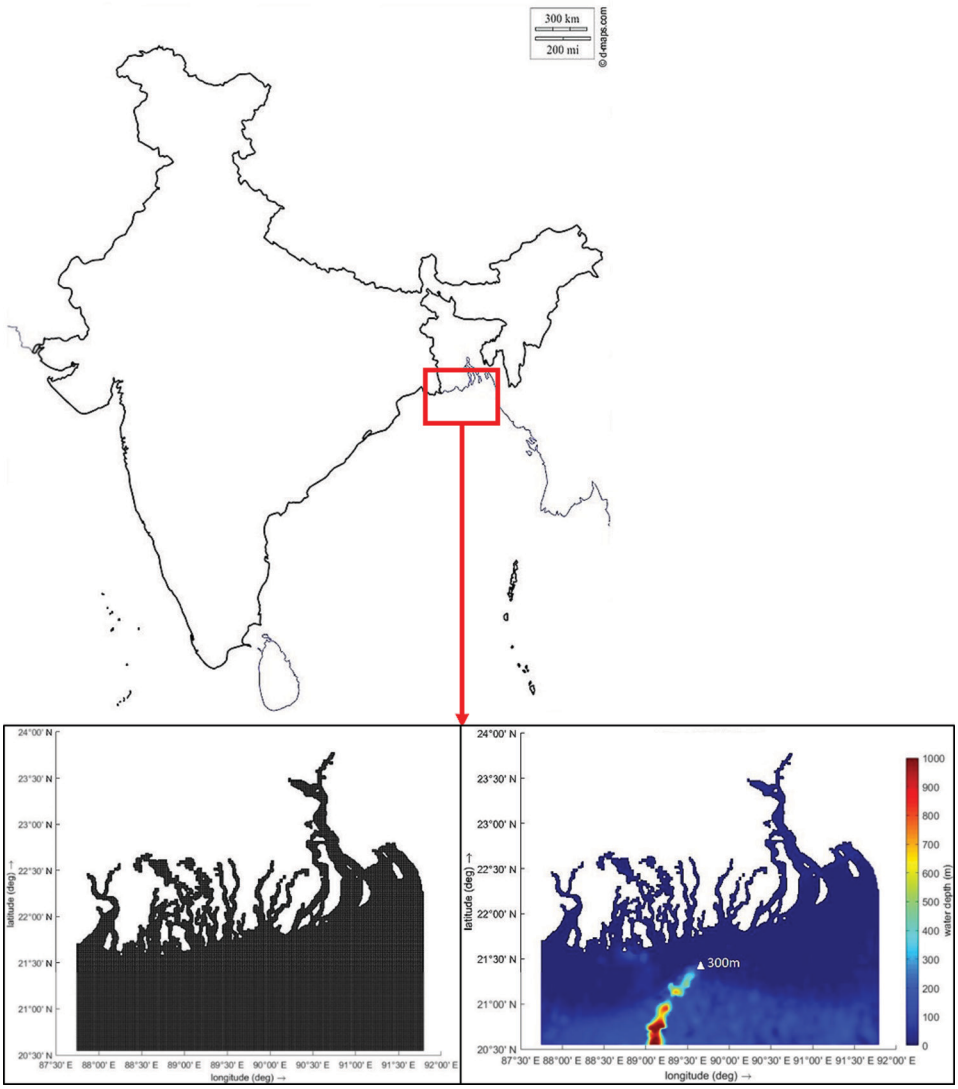

Figure 2. Study area with domain grid and bathymetry.

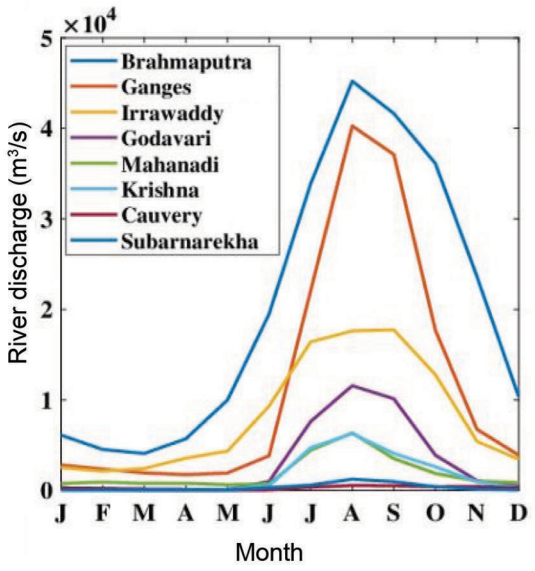

Figure 3. Monthly variability of river discharge into the BoB[45,46].

The grid generation and bathymetry generation were done using the Delft Dashboard. The simulation was done from 1 January 2018 to 31 October 2018 at 120 min intervals. The 11 tidal constituents were imported from the TPXO 7.1 global tidal model. Table 1 provides detail of mesh and input variables.

Artificial neural network

ANN performs data analysis and manipulation by mimicking the brain of living systems. It is a complex process which makes complete visualization of any dataset possible. When we collect datasets with dependent and independent variables, we can use ANN to form a cause–effect relationship between them.

In this study, ANN was used to examine far shelf current velocities. Figure 4 shows the network set-up. The independent parameters: u_m, v_m are Delft3D velocities at 300 m (89.56°E, 21.33°N); ρ density from Delft3D at the

same grid; u_b, v_b represent basin-scale velocities from OSCAR, say at 2000 m. The target parameters u_t, v_t are the OSCAR (satellite) velocities at 300 m. The thermohaline plumes are a response to rivers and precipitation/evaporation[36].

Multiple linear regression

Multiple linear regression (MLR) is a statistical technique used to predict the outcome of a variable based on the value of two or more variables. The formula for MLR is as follows

$$y_i = \beta_0 + \beta_1 x_{i1} + \beta_2 x_{i2} + \ldots + \beta_p x_{ip},$$

where for $i = 1 \ldots n$ observations, y_i are the dependent variables, x_i the explanatory variables, β_0 the y-intercept (constant term) and β_p is the slope coefficients for each explanatory variable.

Results and discussion

The correlation coefficient (R) and root mean square error (RMSE) were estimated to evaluate the accuracy and performance of the network. The continental shelf region in the northern BoB is divided into near shelf and far shelf on the basis of depth. Up to 50 m depth, the tides and local winds strongly influence the movement of the freshwater plume, which is the near shelf region. Beyond 50 m and up to 500 m, where the flow is driven mainly by the deep ocean waters and salinity-driven velocity patterns, is the far shelf.

Sumangala[36] and Warrior[37], reported that the Delft3D output results containing depth-averaged velocities in the near shelf region showed good similarity with the OSCAR velocity with good R values of 0.8 and 0.7 for u and v velocities respectively (Figure 5 *a* and *b*), ascertaining the dominance of tides and local winds. Whereas, Figure 6 *a* and *b* shows that the R value is low and RMSE values are high (0.3–0.4 m/s), implying that Delft3D is not a suitable simulation method to reproduce the far shelf phenomenon.

As mentioned previously, from 50 to 500 m isobaths, using model-velocity parameters alone is insufficient to study freshwater plumes in this region, as basin-scale velocities are more dominant than tides. Due to this error in Delft3D, it is customary to use models like ROMS to study physical processes. An alternative is to augment-Delft3D with ANN to improve coastal predictions.

The data having inputs (Delft3D velocity outputs, density, open-basin velocities) and the target data (OSCAR velocity) were divided into training and testing using the train–test split from the Scikit-learn library[38]. While 80% of the data was used for training, 20% was used for testing. Random Search class from Keras Tuner was used for hyperparameter tuning (layers, neurons, learning rate) of the model. After optimization, the learning rate obtained was 0.001. Table 2 shows the network architecture.

ReLU activation[40] was employed for the hidden layers and the weight initialization technique used was the normal[41]; the output layer contained two neurons with a linear activation function. Adam optimizer was used[42] for reducing the loss function. The training set was divided into 10 k-folds (using the repeated k-fold technique) and trained for 1000 epochs. Each k-fold was used as a validation set. The average loss function, here the mean absolute error, was plotted for the trained and validation sets (Figure 7). An MLR model was also developed with the same dataset. Table 3 lists the MLR coefficients.

Figure 8 is a Taylor diagram for the three models showing which among them is more realistic. Table 4 shows their respective values. It can be seen that RMSE values have decreased and R values have improved when the numerical

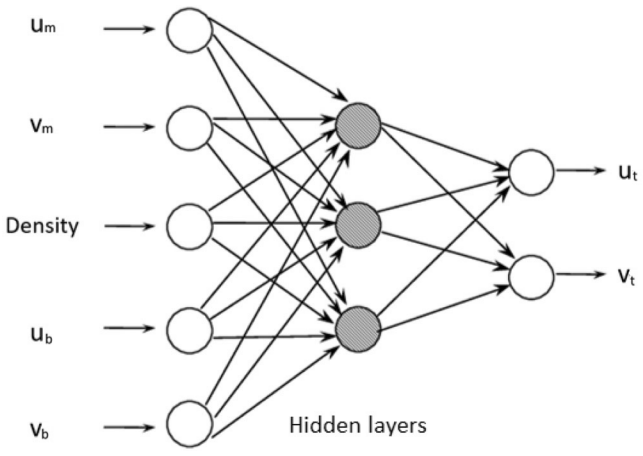

Figure 4. Neural network set-up.

Table 2. Artificial neural network architecture

Hidden layer	Neurons
1	40
2	45
3	30
4	50
5	50
6	40
7	30
8	40
9	30
Output layer	Neurons
1	2

Table 3. Multiple linear regression coefficients for the test set

	B0	B1	B2	B3	B4	B5
u	–386.607	–0.263	0.211	0.376	0.448	0.261
v	335.665	0.074	–0.0134	–0.327	–0.086	0.196

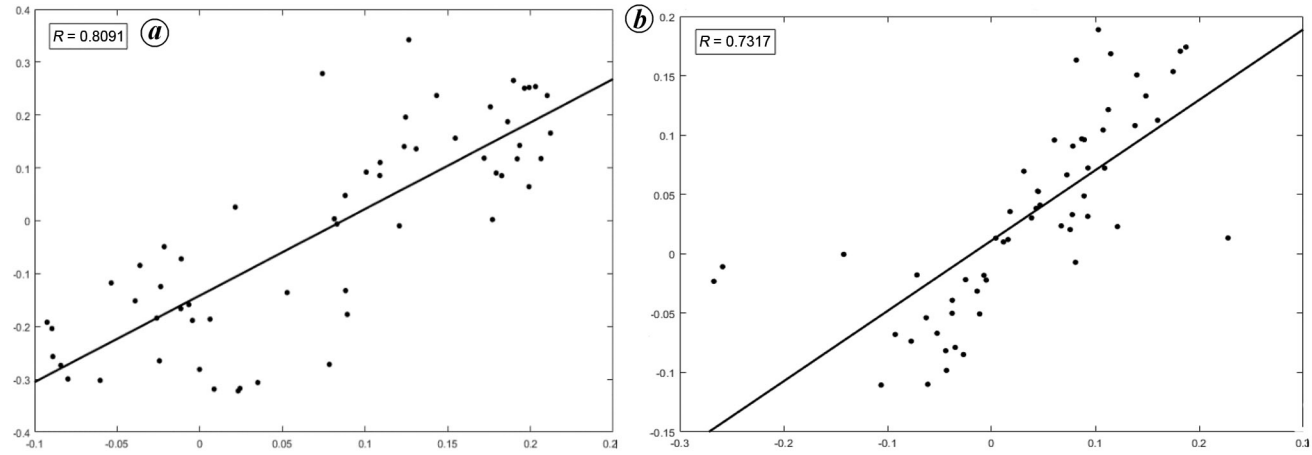

Figure 5. ***a***, *R* for Delft3D versus OSCAR for *u* velocity at 45 m (ref. 36). ***b***, *R* for Delft3D versus OSCAR for *v* velocity at 45 m (ref. 36).

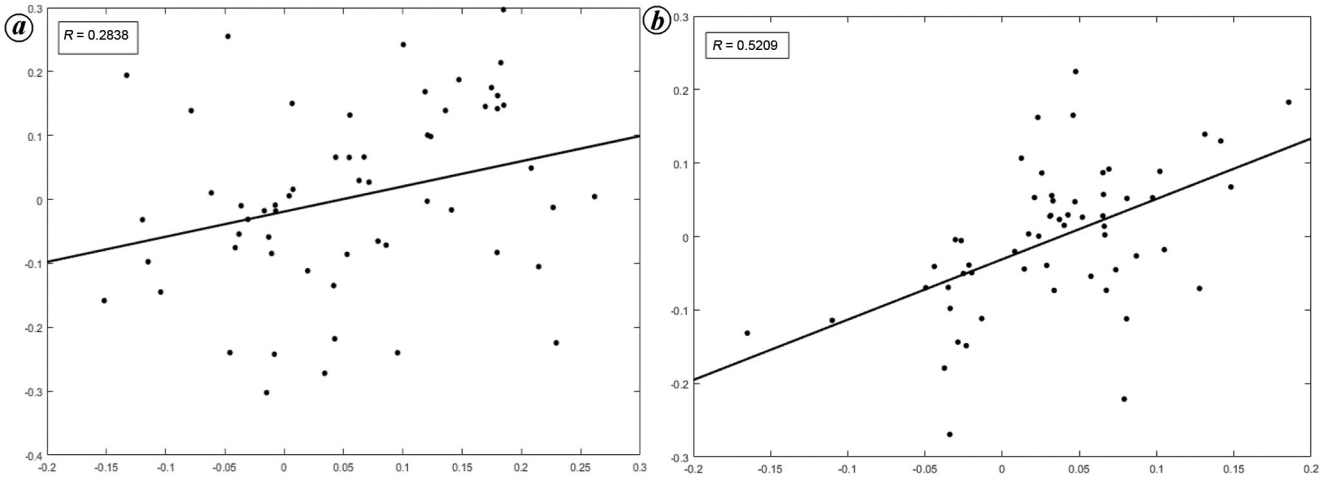

Figure 6. *R* for Delft3D versus OSCAR for *u* velocity at 450 m (ref. 36). ***b***, *R* for Delft3D versus OSCAR *v* velocity at 450 m (ref. 36).

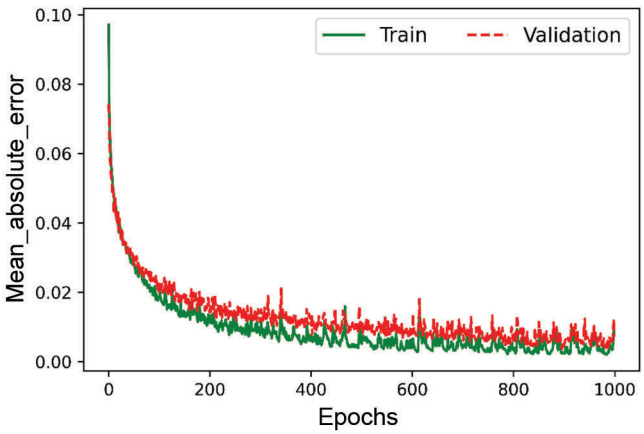

Figure 7. Loss history plot.

model and ANN are combined, compared to the standalone Delft3D and MLR models. This shows that combining the velocities with density in ANN predicts the thermohaline circulation spread by seasonal open-ocean circulation.

Freshwater plume spread – an observational study

The data for sea surface salinity were taken from the National Indian Ocean Atlas (NIOA), which is the climatological atlas for the Indian Ocean region[42,43]. The spread of freshwater plume was observed by isolating 31 practical salinity units (psu) isohaline and considering the same as the limit of saline water.

The location for validating the velocity was chosen at 300 m depth and the results were compared with the ANN results. Figure 9 shows that during March–May, there is the lowest spread of freshwater plume because of less river input to the Bay. The spread increases during the southeast monsoon to a larger area and is associated with higher freshwater flow during the rainy season. During June–August, the freshwater is mainly constrained at the coast

Table 4. Standard deviation (SD), root mean square error (RMSE) and *R* at 300 m

	STD		RMSE		*R*	
Model	*u*	*v*	*u*	*v*	*u*	*v*
Delft3D	0.0609	0.0775	0.1510	0.1252	–0.0026	–0.0186
MLR	0.0787	0.0566	0.1153	0.0815	0.5500	0.5419
Delft3D + ANN	0.1386	0.0966	0.0401	0.0158	0.9579	0.9866

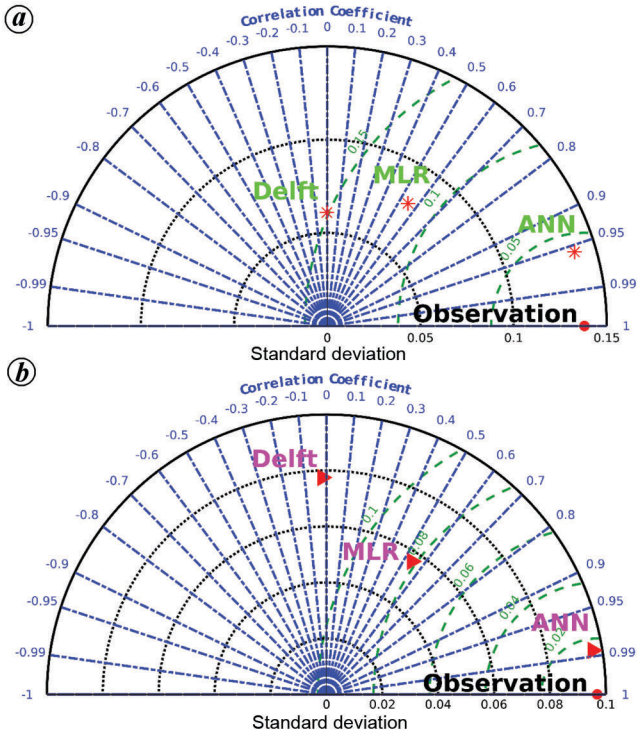

Figure 8. Taylor diagram for (***a***) *u* and (***b***) *v* velocities.

since EICC flows north. By September, EICC starts reversing its direction and started to move south. The extent reaches a maximum by October/November and decreases thereafter. Thus, it can be concluded that the density-driven flow peaks in October/November because of the very high river input and EICC also starts flowing southwards, bringing the freshwater south. Here we see the interaction and feedback between density-driven flow and EICC transport. After December, there is a decrease in the river input and spread.

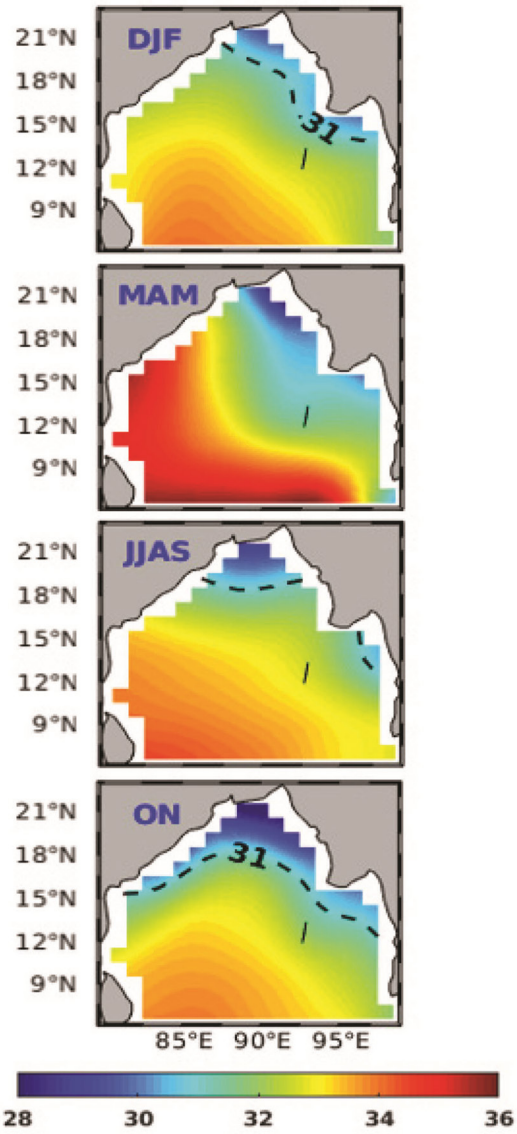

Figure 9. Observations of freshwater plume spread.

Seasonality of open-ocean circulation

The open-ocean features have less influence on the velocities in the near shelf coast region. This can be seen in Figure 4 *a–d* of Sumangala and Warrior[36], where Delft3D simulates the total velocity fields well compared to OSCAR. We observed that the velocity of the freshwater plume from the Delft3D model had a bias of about 0.02 m/s with the OSCAR data. Hence the currents seem to be primarily tide-driven, unlike on the far shelf. The meridional currents change their direction seasonally in response to the rhythm of monsoons. The plume spread in the head BoB follows the current characterized by EICC that flows southwards from November to February, with maximum spread along the coast during November (Figure 9). From March to September, it flows northwards, with

maximum intensity near the coast during April. The spread of the plume varies on a monthly basis according to EICC, which reverses its direction twice a year during November and February. The northeast monsoon is a period of low freshwater outfall from the rivers. Therefore, the density-driven circulation is less; hence the spread is less. Thus, it can be surmised that the freshwater plume (which is density-driven) takes its origin from the river outfall but is also strongly modulated by the seasonally reversing basin-scale circulation (EICC).

Conclusion

This study is an exercise to precisely model the velocity of waters on the far shelf of the head BoB. Flow in the Bay is found to be primarily determined by tidal velocities closer to the coast and by basin-scale, seasonally varying circulation combined with density-driven flows in the far shelf. Though Delft3D is a good hydrodynamic tool for shallow waters, it is unsuitable for predicting far shelf flows. A very high correlation of 0.957 and 0.986 for u and v velocities respectively, using density as an input in ANN indicates that Delft3D coupled with ANN predicts the freshwater plume spread and its velocity more accurately compared to the numerical model alone.

The density of waters in far shelf of the BoB is mainly determined by the freshwater and thus the low-saline water flow is the primary driver. The prediction of flow is a complicated phenomenon with the combined interactions of many features like topographic, wind-induced, climatic phenomena and various types of waves, for which augmenting a numerical model with ANN will give an advanced level of accuracy and computational clarity.

1. Burchard, H., Petersen, O. and Rippeth, T. P., Comparing the performance of the Mellor–Yamada and *k–e* two-equation turbulence models. *J. Geophys. Res.*, 1998, **103**(C5), 10543–10554.
2. Burchard, H. and Petersen, O., Models of turbulence in the marine environment – a comparative study of two-equation turbulence models. *J. Mar. Syst*., 1999, **21**(1–4), 29–53.
3. Rao, R. and Sivakumar, R., Seasonal variability of sea surface salinity and salt budget of the mixed layer of the North Indian Ocean. *J. Geophys. Res.*, 2003, **108**(C1), 9–14.
4. Charhate, S. B., Deo, M. C. and Sanilkumar, V., Soft and hard computing approaches for real–time prediction of currents in a tide-dominated coastal area. *J. Eng. Marit. Environ*., 2007, **221**, 121–130.
5. Rumelhart, D. E., Hinton, G. E. and Williams, R. I., Learning internal representations by error propagation. In *Parallel Distributed Processing* (eds Rumelhart, D. E. and McClelland, J. L.), Cambridge, MIT, USA, 1986, 241–250.
6. Wasserman, P. D., *Advanced Methods in Neural Computing*, Van-Nostrand Reinhold, India, 1993, p. 255.
7. Bose, N. K. and Liang, P., *Neural Network Fundamentals with Graphs, Algorithms and Applications*, McGraw-Hill, 1996, p. 478.
8. Londhe, S. N. and Panchang, V., One-day wave forecasts-based on Artificial Neural Networks. *J. Atmosp. Ocean. Technol*., 2006, **23**, 904–910.
9. Makarynskyy, O., Improving wave predictions with artificial neural networks. *Ocean Eng.*, 2004, **31**, 709–724.
10. Lee, T. L., Jeng, D. S. and Zhang, G. H., Neural network modelling for estimation of scour – depth around bridge piers. *J. Hydrodyn.*, 2007, **19**, 378–386.
11. Cox, D. T., Tissot, P. and Michaud, P., Water level observations and short-term predictions including meteorological events for entrance of Galveston Bay, Texas. *J. Waterw. Port, Coast. Ocean Eng. Div.*, 2002, **128**, 21–29.
12. Churnside, J. H., Stermitz, T. A. and Schroeder, J. A., Temperature profiling with neural network inversion of microwave radiometer data. *J. Atmos. Ocean. Technol*., 1994, **11**, 105–109.
13. Kretzschmar, R., Eckert, P., Cattani, D. and Eggimann, F., Neural network classifiers for local wind prediction. *J. Appl. Meteorol*., 2004, **43**, 727–738.
14. Lee, T. L. and Jeng, D. S., Application of artificial neural networks in tide forecasting. *Ocean Eng*., 2002, **29**, 1003–1022.
15. More, A. and Deo, M. C., Forecasting wind with neural networks. *Mar. Struct.*, 2003, **16**, 35–49.
16. Kambekar, A. R. and Deo, M. C., Estimation of group pile scour using neural networks. *Appl. Ocean Res*., 2003, **25**, 225–234.
17. Deo, M. C., Artificial neural networks in coastal and ocean engineering. *Indian J. Geo-Mar. Sci.*, 2010, **39**, 589–596.
18. Dwarakish, G. S., Shetty, R. and Usha, N., Review on applications of neural network in coastal engineering, *Int. J. Artif. Intell. Syst. Mach. Learn*., 2013, **5**, 324–331.
19. Reddy, N. B., Kuntoji, G., Rao, S., Manu, D. and Mandal, S., Prediction of wave transmission using ANN for submerged reef of tandem breakwater. *Int. J. Innov. Res. Sci., Eng. Technol*., 2016, **5**, 137–142.
20. Gopinath, D. I. and Dwarakish, G. S., Real-time prediction of waves using neural networks trained by particle swarm optimization, *Int. J. Ocean Climate Syst*., 2016, **7**, 70–79.
21. Adhikary, S., Chaturvedi, S. K., Banerjee, S. and Basu, S., Dependence of physiochemical features on marine chlorophyll analysis with learning techniques, advances in environment engineering and management. In Proceedings in Earth and Environmental Sciences. Springer, Cham, 2021.
22. Dauji, S., Deo, M. C. and Bhargava, K., Prediction of ocean currents with artificial neural networks, *ISH J. Hydraul. Eng*., 2015, **21**, 14–27.
23. Wu, K. K., *Neural Networks and Simulation Methods*, Marcel Decker, New York, USA, 1994, pp. 35–52.
24. Sivakumar, B. and Berndtsson, R., *Advances in Data-Based Approaches for Hydrologic Modelling and Forecasting*, World Scientific Publishing Company, Singapore, 2010, pp. 25–35.
25. Jain, P. and Deo, M. C., Neural networks in ocean engineering. *Int. J. Ships Offshore Struct.*, 2006, pp. 25–35.
26. Sarma, V. *et al.*, Sources and sinks of CO_2 in the west coast of Bay of Bengal. *Chem. Phys. Meteorol.*, 2012, **64**, 40–65.
27. Discharge of selected rivers of the world, Volume II (Part II), UNESCO, 1969.
28. Shetye, S. *et al.*, Hydrography and circulation in the western Bay of Bengal during the northeast monsoon. *J. Geophys. Res.: Oceans*, 1996, **101**, 14011–14025.
29. Krishna, V. and Sastry, J., Surface circulation over the shelf off the east coast of India during the southwest monsoon. *India. J. Geo.-Mar. Sci.*, 1985, **14**, 62–65.
30. Krishna, S. and Warrior, H., Seasonal variability of circulation along the north–east coast of India using Princeton ocean model. In Proceedings of Fourth International Conference in Ocean Engineering, Singapore, Springer, 2019, pp. 733–748.
31. Warrior, H. and Carder, K., Production of hypersaline pools in shallow basins by evaporation, *Geophys. Res. Lett*., 2005, **32**, 1320–1333.
32. Bonjean, F. and Lagerloef, G. S. E., Diagnostic model and analysis of the surface currents in the tropical pacific ocean. *J. Phys. Oceanogr*., 2002, **32**, 2938–2954.

33. Shetye, S. R. and Shenoi, S. S. C., Seasonal cycle of surface circulation in the coastal North Indian Ocean. *Proc. Indian Acad. Sci*., 1988, **7**, 53–62.
34. Rao, R. R., Molinari, R. L. and Festa, J. F., Surface meteorological and near surface oceanographic atlas of the tropical Indian Ocean, NOAA-Tech. Memo. AOML-69, 1991
35. Aydogan, B., Berna Ayat, M. N., Ozturk, E., Cevik, O. and Yuksel, Y. I., Current velocity forecasting in straits with artificial neural networks, a case study: Strait of Istanbul. *Ocean Eng.*, 2010, **37**, 443–453.
36. Sumangala, D. and Warrior, H., Coastal modelling incorporating artificial neural networks for improved velocity prediction. *ISH J. Hydraul. Eng.*, 2020, **28**(sup1), 1–11.
37. Warrior, H. and Carder, K., An optical model for heat and salt budget estimation for shallow seas. *J. Geophys. Res.: Oceans*, 1991, **112**, 2825–2830.
38. Pedregosa, F. *et al*., Scikit-learn: machine learning in Python. *J. Mach. Learn. Res.*, 2011, **12**, 2825–2830.
39. O'Malley, T., Bursztein, E., Long, J., Chollet, F., Jin, H. and Invernizzi, L., Keras Tuner, 2019; https://github.com/keras-team/keras-tuner
40. Agarap, A. F., Deep learning using rectified linear units. arxiv2-8; 2018; pre-print at https://arxiv.org/abs/1803.08375.
41. He, K., Zhang, X., Ren, S. and Sun, J., Delving deep into rectifiers: surpassing human-level performance on image net classification. In IEEE International Conference on Computer Vision, Raleigh, 2015, pp. 1026–1034.
42. Diederik, P., Kingma, Diederik, P. and Jimmy, B., Adam: a method for stochastic optimization. CoRR, abs/1412.6980, 2014.
43. Chatterjee, A. *et al.*, A new atlas of temperature and salinity for the North Indian Ocean. *J. Earth Syst. Sci*., 2012, **121**, 559–593.
44. Joshi, A. P., Chowdhury, R. R., Kumar, V. and Warrior, H. V., Configuration and skill assessment of the coupled biogeochemical model for the carbonate system in the Bay of Bengal. *Mar. Chem*., 2020, **226**, 103871.
45. Dai, M. *et al.*, Why are some marginal seas sources of atmospheric CO_2? *Geophys. Res. Lett*., 2013, **40**, 2154–2158.
46. Dai, A., Qian, T., Trenberth, K. E. and Milliman, J. D., Changes in continental freshwater discharge from 1948 to 2004. *J. Climate*, 2009, **22**, 2773–2792.

Received 30 August 2021; re-revised accepted 26 April 2022

doi: 10.18520/cs/v123/i1/73-80